


On the mechanisms of surface microdischarge plasma treatment of onychomycosis: Penetration, uptake, and chemical reactions

Zilan Xiong  | Renjie Huang | Yu Zhu | Kang Luo | Mengqi Li | Zhenping Zou | Rui Han

State Key Laboratory of Advanced Electromagnetic Engineering and Technology, Huazhong University of Science and Technology, Wuhan, Hubei, China

Correspondence

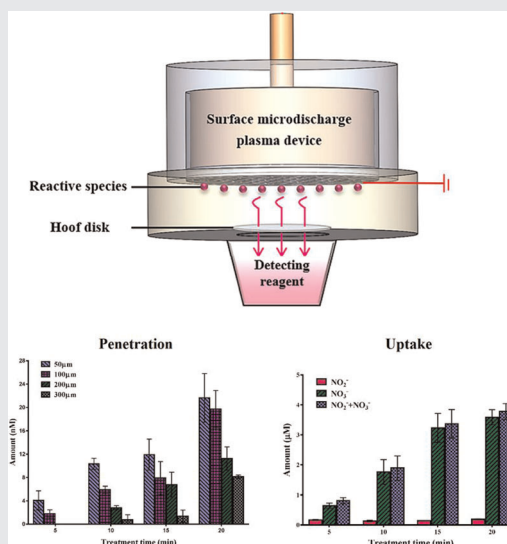
Zilan Xiong, State Key Laboratory of Advanced Electromagnetic Engineering and Technology, Huazhong University of Science and Technology, West 9 building, School of Electrical and Electronic Engineering, 1037 Luoyu Road, Wuhan, Hubei 430074, China.
Email: zilanxiong@hust.edu.cn

Funding information

National Natural Science Foundation of China, Grant/Award Number: 51907076

Abstract

Despite becoming increasingly established as a treatment technique, the mechanism underlying the plasma treatment of onychomycosis has yet to be elucidated. Here, we focus on the interactions between the nail plate and a surface microdischarge plasma, including penetration, uptake, and chemical reactions. Results show that long-lived gaseous species from plasma can penetrate the nail plate effectively and are primarily responsible for the instantaneous antionychomycosis effect. The amount of uptake far exceeded that of penetration. Attenuated total reflection-Fourier-transform infrared spectroscopy and X-ray photoelectron spectroscopy results show that antimicrobial compounds form on the nail surface. Combined with the uptake of active species in the nail plate, these antimicrobial compounds may inhibit microorganism growth, thereby promoting long-term protection against onychomycosis.



KEYWORDS

chemical reaction, dielectric barrier discharges (DBD), onychomycosis, penetration, uptake

Cold atmospheric plasmas (CAPs) have shown great potential in biomedical applications, such as cancer treatment, dentistry, chronic wound healing, dermatology, and cell differentiation.^[1-4] Recently, clinical trials involving commercially available plasma devices have been conducted on patients, yielding remarkable results.^[5] Plasmas can create

highly reactive species, such as NO, NO₂, OH, H₂O₂, O, and photons. On the contrary, such species can effectively inactivate microorganisms or mammalian cancer cells; nevertheless, they can also enhance normal cell proliferation or differentiation.^[6,7] Recent research modeling murine cancers have reported that plasma can even stimulate the immune

system and prompt immunocytes to attack target tumors.^[8] Although the underlying mechanisms dictating plasma interaction with cells, tissues, and substrates are studied and analyzed by research groups worldwide, they are yet to be fully understood.^[9–11] However, reactive oxygen and nitrogen species (ROS; RNS) created by plasma are believed to play a major role in these processes, while electrons, charged particles, and electric field effects may also contribute to plasma-target interactions, depending on the plasma source configuration, the physical conditions used, and the processing mode.

Among plasma-related biomedical applications, the treatment of onychomycosis is a nascent technique that has received increasing attention recently. Onychomycosis is a fungal infection of the nail, with such infections estimated to affect 10% of adults worldwide.^[12] The global onychomycosis therapeutics market is projected to expand at a compound annual growth rate of 7.6% from 2018 to 2026, and reach a value of \$6741.6 million by the end of this period.^[13] Unlike ordinary nail surface infections, the microorganisms involved in onychomycosis usually live within or under the nail plate. The nail plate consists predominantly of keratin, which contains 18 kinds of amino acid and shows high stability and low solubility owing to the disulfide bridges between cysteine amino acid residues.^[14,15] Owing to its high keratin content and composition of tightly packed dead cells, the nail plate exhibits poor permeability, which limits the effectiveness of traditional topical therapies.^[16] Additionally, antifungal therapies involving oral medication have also been proven to have limited success, with their disadvantages, including drug interactions, side effects, and the need for high financial and time investments, whereas they have also been considered to increase the resistance to antifungal agents.^[17,18] Consequently, there is a great demand for new methods that can treat onychomycosis more efficiently.

Previously, we reported a remarkable in vitro anti-onychomycosis effect using three different CAPs.^[19] A 2–6 log reduction of both *Escherichia coli* and *Trichophyton rubrum* located on the ventral side of a sealed nail plate was achieved within 20–45 min of CAP treatment. Bulson et al.^[20] also investigated the antifungal effect of applying pulsed dielectric barrier discharge to treat onychomycosis for a human nail model. The authors reported that *Candida albicans* and *Trichophyton mentagrophytes* were effectively inactivated by short-term plasma treatment. Alternatively, Lipner et al.^[21] used a CAP device to conduct a preliminary study on the effect of plasma treatment of onychomycosis for 10 patients and evaluated the safety of the procedure. They found that more than 50% of the patients were clinically cured without experiencing side effects. However, these studies focused mainly on discovering the preliminary plasma-induced antionychomycosis effect both in vitro and

in vivo; however, the mechanisms by which plasma interacts with the nail plate and the mechanisms underlying plasma-induced onychomycosis resistance are not clear. The anti-onychomycosis effects reported for in vitro nail models and in vivo clinical trials encompass both instantaneous antimicrobial processes involving the nail plate and long-term microorganism inhibition posttreatment. Therefore, in this study, we investigated possible mechanisms active in the indirect CAP treatment of onychomycosis, including gas penetration, uptake, and the chemical reactions between plasma and the nail plate.

The CAP device used in this study was a surface microdischarge (SMD) plasma source, with the details of the experimental setup depicted in Figure 1a. The powered electrode was made of copper with a diameter of 20 mm and a thickness of 5 mm and was covered by polytetrafluoroethylene. A woven wire mesh of stainless steel (diameter: 0.5 mm, mesh density: 4×4 cells cm^{-2}) was used as the ground electrode. A ceramic sheet (diameter: 40 mm, thickness: 1 mm) was used as a dielectric layer between the copper sheet and the woven wire mesh. Further details on the device structure can be found in Reference [22]. The SMD device was driven by a high-voltage AC power supply (CTP-2000K; Corona Lab), which was operated under V_{p-p} 11 kV and 8 kHz using ambient air as the working gas. The applied voltage and current waveforms were measured using high-voltage (P6015A; Tektronix) and current probes (P6585; Pearson), respectively, whereas the voltage across the capacitor was detected using a differential voltage probe (P5200A, 50 MHz/1300 V; Tektronix). All probes were connected to an oscilloscope (MDO3034, 350 MHz; Tektronix). The voltage and current waveforms are shown in Figure 1b. The discharge power was measured using the Lissajous method and was fixed at 8 W. The gas-phase products created under these conditions were detected via Fourier-transform infrared spectroscopy (FTIR) spectroscopy (VERTEX 70; Bruker), as shown in Figure 1c. It has been reported that the SMD could operate in two main modes according to the dominating products by varying the input power density.^[23] Under low input power density, the gaseous products are dominated by O_3 , and this was called O_3 mode. The other one is named NO_x mode when operating at higher input power density with NO_x as the dominating product. The FTIR spectrum clearly shows that the SMD plasma source was operating in NO_x mode during this investigation; therefore, the dominant products of the active species (other than O_3) were NO_x . More specifically, the main gas-phase products in NO_x mode were NO , NO_2 , and N_2O , whereas the water vapor in the ambient air gives rise to H_2O_2 .^[24]

The antimicrobial effect through the nail plate was evaluated to show the instantaneous effects of the treatment. The bacterial experiments used in this involved the pathogen *Pseudomonas aeruginosa* (CGMCC 1.15148), which was

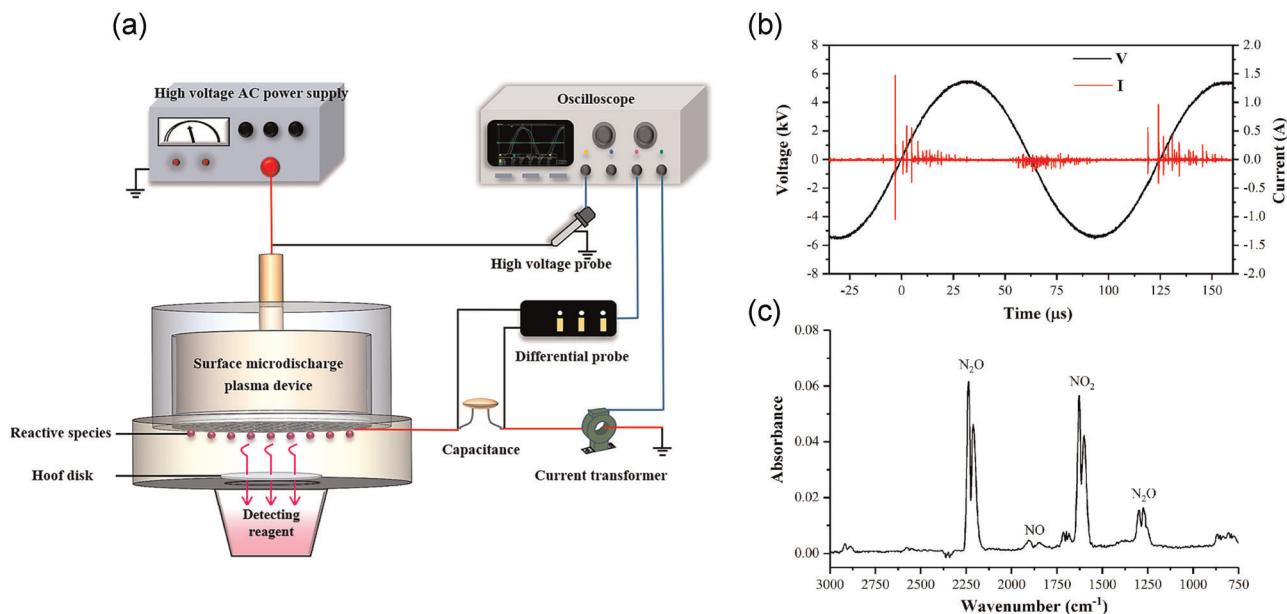


FIGURE 1 (a) Experimental setup; (b) applied voltage and current waveform; (c) Fourier-transform infrared spectrum measurement of the gas-phase products in NO_x mode

procured from the China General Microbiological Culture Collection Center. *P. aeruginosa* is a versatile pathogen associated with a variety of human infections, especially in immunosuppressed individuals and patients in intensive care units. Some infections, such as folliculitis, green nail, and hot foot syndromes, are common in community settings.^[25] Samples of *P. aeruginosa* were prepared following a similar approach as in our previous work.^[19] First, *P. aeruginosa* was grown in Nutrient Broth medium, obtaining approximately 10^9 colony-forming units per milliliter (CFU ml^{-1}). Next, suspensions of *P. aeruginosa* were pelleted in 50- μl aliquots via centrifugation at 7000 rpm. Before treatment, *P. aeruginosa* was spread and dried on the surface of a bovine hoof slice for use.

The nail model used in this investigation was made from the bovine hoof, a well-recognized surrogate for human nails.^[26] Moreover, it has been reported that the difference in the mean surface pore size between bovine hooves and human nails is negligible.^[27] The bovine hoof was purchased from a slaughterhouse and was cut, shaped, and ground into 1.5-cm-diameter slices of different thicknesses. To measure the instantaneous antimicrobial effect and gas product penetration through the nail plate, a slice of the bovine hoof was mounted centrally to separate the upper and lower chambers (Figure 1a). When conducting the antimicrobial experiments, the side with *P. aeruginosa* was facing the lower chamber and called the backside. The edge of the hoof slice was sealed with an O-ring and vacuum resin to eliminate gas leakage into the lower chamber. Therefore, the effective diameter for gas penetration was 1 cm.

Additionally, the separation distance between the ground mesh and the nail plate surface was fixed at 5 mm.

Plasma was then applied to the top of the hoof slice for a range of durations to represent different treatment times. Each treatment time was tested for six samples. After treatment, each hoof slice was placed in a container with 1 ml phosphate-buffered saline (PBS) and vortexed for 10 min to wash the cells from the hoof plate. Next, the suspension was serially diluted (six dilutions, each by a factor of 10) using sterile PBS. At each dilution stage, 20 μl of the solution was transferred onto an agar plate and incubated overnight at 37°C. As in our previous study, the antimicrobial effect of each treatment was assessed by calculating both the % reduction and the logarithmic (log) reduction factor (RF) using $\text{RF} = \log_{10} (\text{CFU}_{\text{untreated plate}}) - \log_{10} (\text{CFU}_{\text{treated plate}})$; the antimicrobial results are shown in Figure 2. The survival of *P. aeruginosa* decreased as treatment time increased. Notably, the log reduction of the 20-min plasma treatment was ~ 2 , showing similarity with our previous results.^[19] After 30 min of treatment, the average log reduction was ~ 5 , demonstrating the excellent instantaneous antimicrobial performance of plasma treatment through the hoof plate.

For nail plates with a thickness of hundreds of microns, only long-lived species from the gas-phase products of SMD treatment can penetrate through the nail plate to reach the backside. Therefore, we measured the penetration of possible long-lived species through nail plates with different thicknesses as a function of treatment time. Penetration measurements were performed for thicknesses of 50, 100, 200, and 300 μm . A container with a 2-ml mixture of water and specific reagents was

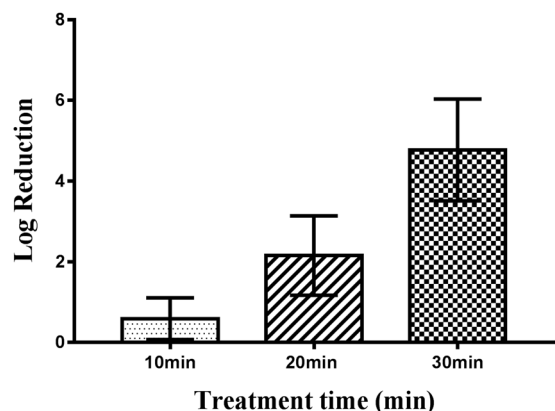


FIGURE 2 Instantaneous antimicrobial effect caused by plasma treatment on the backside of bovine hoof slices for various treatment times

placed under the nail plate to measure the penetration of reactive species. Because the mixed solution was immediately beneath the sealed nail plate, if the penetration of long-lived reactive species through the nail plate was detected by the mixed solution, it would change from colorless to a related color. The possible long-lived reactive species capable of penetrating the nail plate include NO , NO_2 , and H_2O_2 ; however, we did not detect either NO_3^- or H_2O_2 . Only NO_2^- was detected in the mixed solution (via the Griess method^[28]). After a period of discharge, the container was removed and the mixture was shaken. Then, the solution was transferred to a cuvette and kept in the dark for 30 min before the UV-Vis absorption spectrum was recorded (absorbance at 540 nm). An NO_2^- concentration control was measured

using an aluminum plate of the same size as the hoof slice. At least three samples were analyzed for each testing point.

Figure 3 shows the NO_2^- concentration in solution (an indicator of reactive species penetrating through the nail plate) as a function of treatment time and nail thickness. As expected, the degree of penetration increases with treatment time and decreases with nail thickness. For 5 min of treatment, no penetration was observed for the 200 and 300- μm nail plates. For the 300- μm plates, penetration began after approximately 10 min and increased to ~ 8 nM after 20 min. These results confirm that the reactive species created by SMD operating in NO_x mode can penetrate through nail plates with thicknesses up to 300 μm using treatment times on the order of tens of minutes. The penetration of reactive species may contribute to instantaneous antimicrobial effects.

As mentioned above, the keratinous nail plate is a porous material, and water sorption in keratinous tissues has been reported.^[29] During the penetration process, reactive species can be taken up by the keratin-based material. Therefore, we also measured the uptake of reactive species by the treated nail plate using the following procedure: (1) The nail plate was placed in 5 ml of PBS immediately after treatment; (2) the nail plate in PBS was soaked for at least 1 h to allow the uptake species to diffuse into the solution (provided uptake occurs, certain species can be detected in solution); (3) the NO_2^- , NO_3^- , and H_2O_2 concentrations were measured using Griess reagent (Sigma-Aldrich), 2,6-dimethylphenol (Sinopharm), and H_2SO_4 -dissolved $\text{Ti}(\text{SO}_4)_2$ solution (Sinopharm) via UV-Vis absorption at 540, 340, and 407 nm, respectively.

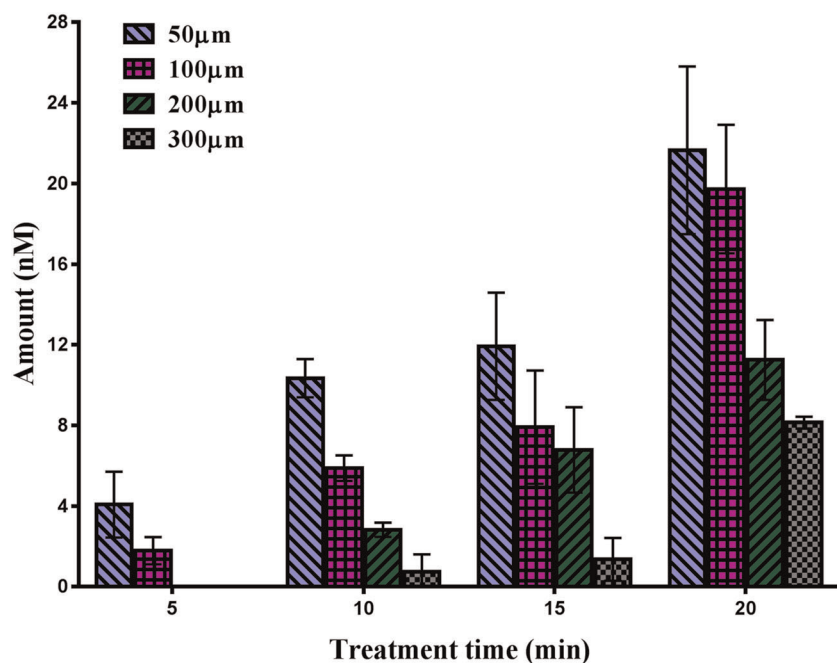


FIGURE 3 Concentration of nitrite in solution (an indicator of NO_x penetrating through the nail plate) as a function of treatment time for different nail thicknesses

The detection method of NO_2^- was the same as that in the penetration experiment above. A more detailed procedure for NO_3^- and H_2O_2 detection could be found in References [30] and [24], respectively. As in the penetration detection, H_2O_2 was not detected in the solution. Figure 4 shows the amount of NO_2^- and NO_3^- uptake by the nail plate as a function of treatment time. The thickness of the nail plate used in this experiment was fixed at $300\ \mu\text{m}$. No NO_2^- or NO_3^- was detected in the control group. As shown in Figure 4, the NO_2^- concentration remained relatively stable as the treatment time changes; however, the amount of NO_3^- increased sharply with treatment time. For the $300\text{-}\mu\text{m}$ -thick nail plates, 20 min of SMD treatment resulted in an NO_3^- uptake approximately 20 times larger than that of NO_2^- . Meanwhile, the amount of NO_2^- detected in the uptake experiment was approximately 25 times higher than that detected in the penetration experiment.

To investigate the interaction between the nail plate and the SMD plasma, attenuated total reflectance-FTIR (ATR-FTIR) and X-ray photoelectron spectroscopy (XPS) measurements were conducted. A clean, dry, untreated sample served as the control for ATR-FTIR (VERTEX 70; Bruker) measurements. Measurements were performed for at least six samples (both for untreated and treated samples). Figure 5a shows ATR-FTIR spectra representing an untreated sample and a sample that underwent 20 min of SMD treatment. Identical amide I ($1650\ \text{cm}^{-1}$), amide II ($1540\ \text{cm}^{-1}$), and NH stretch ($3300\ \text{cm}^{-1}$) bonds are observed in both cases.^[31] Following 20 min of plasma treatment, several new bonds are detected on the surface of the treated sample: N–O stretch at $\sim 823\ \text{cm}^{-1}$, S=O stretch at $\sim 1040\ \text{cm}^{-1}$, N=O (Nitro) at $\sim 1315\text{--}1355\ \text{cm}^{-1}$, S–NO at $1405\text{--}1438\ \text{cm}^{-1}$, and C=O

stretch at $\sim 1722\ \text{cm}^{-1}$.^[32,33] The most obvious change is a significant group bond over $1100\text{--}1480\ \text{cm}^{-1}$, with this region including the related N=O and S–NO bonds. In addition, the presence of S–nitrosothiols (S–NO), which possess antifungal properties, has been reported in acidified nitrite-treated nail plates.^[34] As untreated nail plates are devoid of N=O bonds, this result indicates that oxidation reactions occur between keratin and the NO_x created by SMD plasma.

XPS measurements were performed to investigate the surface changes in greater detail. Nail plates were cleaned and dried before treatment, with the control and treated samples both obtained from the same nail plate. After treatment, the samples were dried overnight in an oven at 85°C before XPS (PHI 5600; Perkin Elmer) measurements were performed. As shown in Figure 5b, the XPS results were consistent with those of ATR-FTIR. The long-range XPS survey clearly presents a new peak at 408 eV, which corresponds to $-\text{NO}_3$ bonding (N1s). In the high-resolution spectra of C1s, N1s, and O1s, new peaks indicating the presence of R–O– NO_2 and $-\text{NO}_3$ on the keratin surface are observed. The same surface-bound $-\text{NO}_3$ has been detected on SMD-treated lipopolysaccharide, polymethyl methacrylate, polypropylene, and polystyrene and likely play a significant role in determining their antibacterial properties.^[35]

As mentioned above, the SMD device was operated in NO_x mode during all experiments, with NO, NO_2 , and H_2O_2 anticipated as long-lived reactive species accordingly. Because the mesh is ground, the plasma cannot make direct contact with the nail surface during treatment. Therefore, reactive species created by the SMD plasma are the predominant factor in determining onychomycosis resistance.

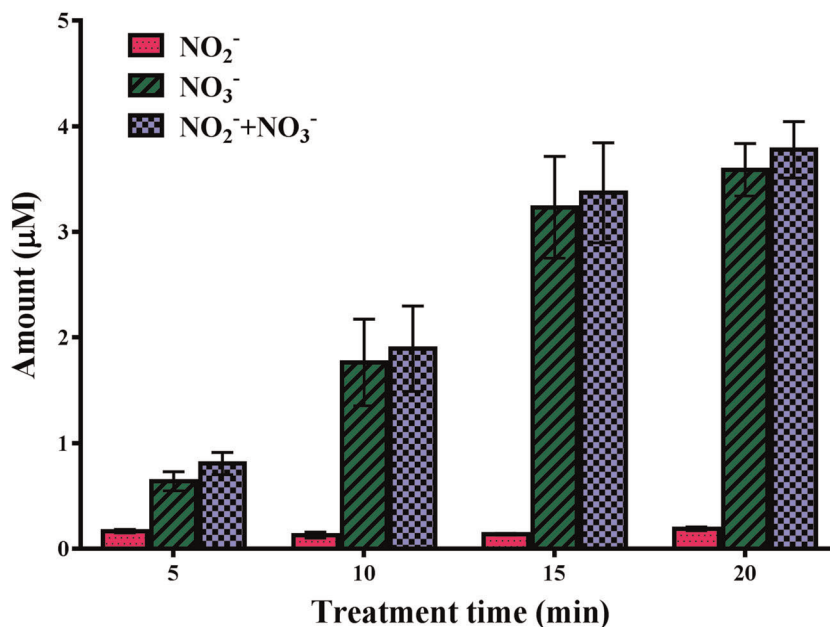


FIGURE 4 Concentrations of NO_2^- and NO_3^- (indicators of active species uptake) in the nail plate as a function of treatment time

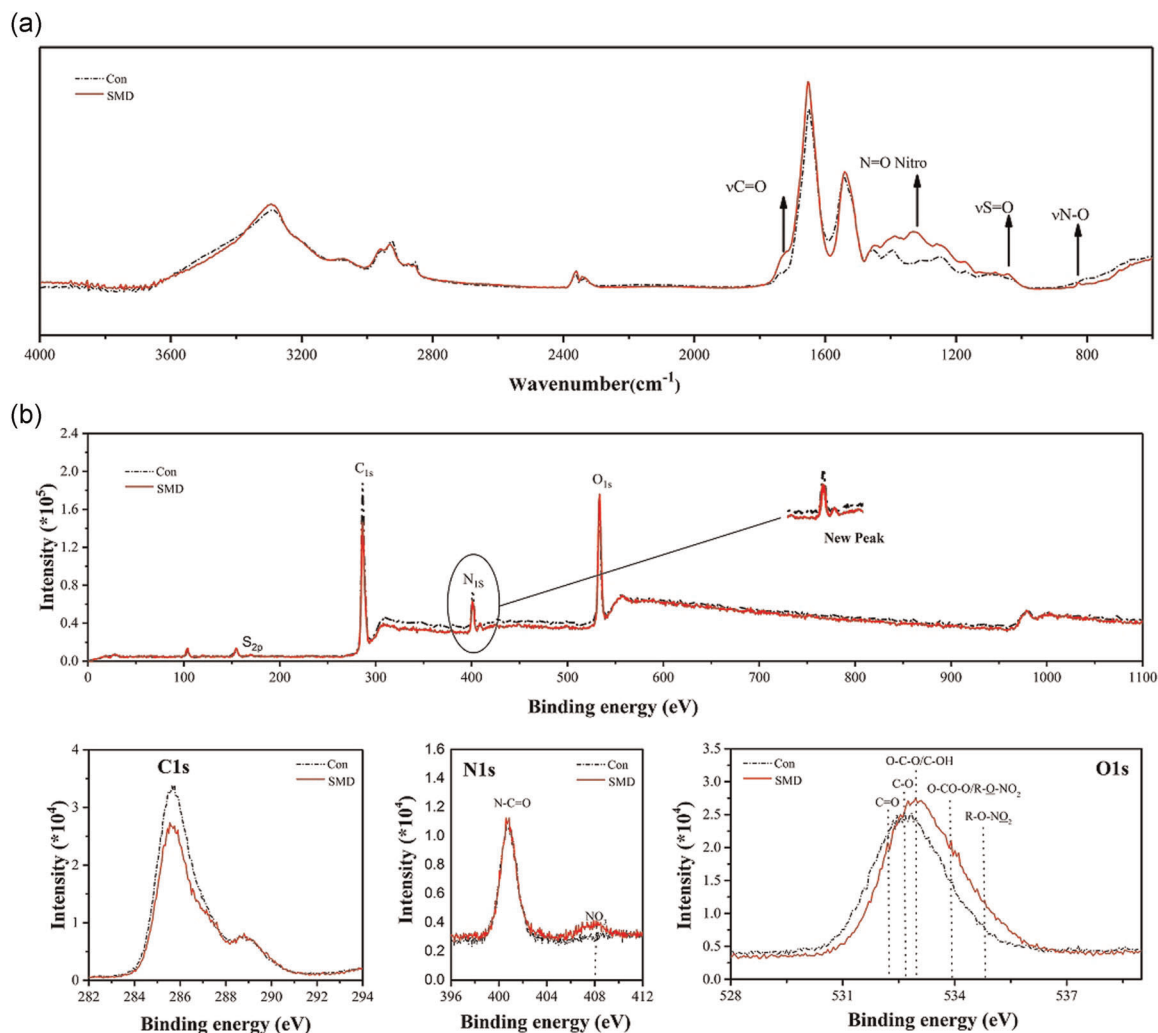
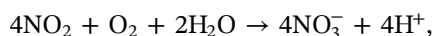
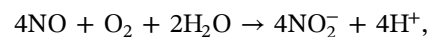


FIGURE 5 Surface characteristics of untreated and surface microdischarge (SMD)-treated (for 20 min) nail plates measured by attenuated total reflectance-Fourier-transform infrared spectroscopy (ATR-FTIR) and X-ray photoelectron spectroscopy (XPS). (a) The ATR-FTIR spectra show that several new peaks emerge after SMD treatment; (b) Large-scale survey and high-resolution spectra of C1s, N1s, and O1s bonding obtained using XPS

Notably, NO_2^- , NO_3^- , and H_2O_2 can be formed in water through the following reactions^[36]:



From the penetration results, it is evident that long-lived NO_2 and NO could penetrate the nail plate, arrive at the backside, and form NO_2^- in the detection solution, thus contributing to the instantaneous antimicrobial effects induced by the SMD treatment of onychomycosis. During the penetration process, a relatively large amount of reactive species was taken up by the nail plate and trapped in its porous structure. These reactive species

could work continuously to combat microorganisms within the nail plate, acting in a manner analogous to a drug-delivery system and leading to long-term onychomycosis protection. Moreover, during the penetration and uptake processes, the reactive species could also interact with keratinous material to form similar antimicrobial compounds within the nail plate as on the surface. These antimicrobial compounds may also contribute to long-term antionychomycosis properties.

In summary, CAP treatment is an effective and promising technique for onychomycosis therapy. This study demonstrates the mechanisms underlying SMD plasma (in NO_x mode) treatment of onychomycosis. It was established that the long-lived reactive species NO and NO_2 can effectively penetrate nail plates and play an active role in instantaneous antimicrobial effects on the backside of the plate. The degree of reactive species uptake by the nail plate

far exceeds the degree of penetration, with these active species working continuously within the nail plate to sustain their long-term microbial resistance. Antimicrobial compounds were found on the keratin surface following SMD treatment and also formed inside the nail plate during the penetration and uptake processes. Therefore, the penetration, uptake, and antimicrobial compound formation involving reactive species all contribute to the antionychomycosis effects induced by SMD plasma.

ACKNOWLEDGMENT

The authors are grateful for financial support from the National Natural Science Foundation of China (No. 51907076).

DATA AVAILABILITY STATEMENT

The data that supports the findings of this study are available within the article.

ORCID

Zilan Xiong  <http://orcid.org/0000-0003-1095-3959>

REFERENCE

- [1] S. Iseki, K. Nakamura, M. Hayashi, H. Tanaka, H. Kondo, H. Kajiyama, H. Kano, F. Kikkawa, M. Hori, *Appl. Phys. Lett.* **2012**, *100*, 113702.
- [2] V. Arora, *Dentistry* **2013**, *4*.
- [3] J. Heinlin, G. Morfill, M. Landthaler, W. Stolz, G. Isbary, J. L. Zimmermann, T. Shimizu, S. Karrer, *J. Dtsch. Dermatol. Ges.* **2010**, *8*, 968.
- [4] Z. Xiong, S. Zhao, X. Mao, X. Lu, G. He, G. Yang, M. Chen, M. Ishaq, K. Ostrikov, *Stem Cell Res.* **2014**, *12*, 387.
- [5] T. vonWoedtke, H. R. Metelmann, K. D. Weltmann, *Contrib. Plasma Phys.* **2014**, *54*, 104.
- [6] A. B. Shekhter, V. A. Serezhenkov, T. G. Rudenko, A. V. Pekshev, A. F. Vanin, *Nitric oxide* **2005**, *12*, 210.
- [7] J. Liebmann, J. Scherer, N. Bibinov, P. Rajasekaran, R. Kovacs, R. Gesche, P. Awakowicz, V. Kolb-Bachofen, *Nitric Oxide Biol. Chem.* **2011**, *24*, 8.
- [8] K. Mizuno, K. Yonetamari, Y. Shirakawa, T. Akiyama, R. Ono, *J. Phys. D: Appl. Phys.* **2017**, *50*, 12LT01.
- [9] X. Lu, T. Ye, Y. Cao, Z. Sun, Q. Xiong, Z. Tang, Z. Xiong, J. Hu, Z. Jiang, Y. Pan, *J. Appl. Phys.* **2008**, *104*, 053309.
- [10] E. Bormashenko, G. Whyman, V. Multanen, E. Shulzinger, G. Chaniel, *J. Colloid Interface Sci.* **2015**, *448*, 175.
- [11] D. Dobrynin, G. Fridman, G. Friedman, A. Fridman, *New J. Phys.* **2009**, *11*, 115020.
- [12] D. P. Westerberg, M. J. Voyack, *Am. Fam. Physician* **2013**, *88*, 762.
- [13] Persistence Market Research 2018. <https://www.giiresearch.com/report/pMrs683955-global-market-study-on-dermatophytichomycosis.html>
- [14] A. N. Parbhu, W. G. Bryson, R. Lal, *Biochemistry* **1999**, *38*, 11755.
- [15] M. Feughelman, *J. Appl. Polym. Sci.* **2002**, *83*, 489.
- [16] M. V. Saner, A. D. Kulkarni, C. V. Pardeshi, *J. Drug Target* **2014**, *22*, 769.
- [17] M. A. Repka, J. O'Haver, C. H. See, K. Gutta, M. Munjal, *Int. J. Pharm.* **2002**, *245*, 25.
- [18] E. G. Evans, *J. Am. Acad. Dermatol.* **1998**, *38*, S32.
- [19] Z. Xiong, J. Roe, T. C. Grammer, D. B. Graves, *Plasma Processes Polym.* **2016**, *13*, 588.
- [20] J. M. Bulson, D. Liveris, I. Derkatch, G. Friedman, J. Geliebter, S. Park, S. Singh, M. Zemel, R. K. Tiwari, *Mycoses* **2020**, *63*, 225.
- [21] S. R. Lipner, G. Friedman, R. K. Scher, *Clin. Exp. Dermatol.* **2017**, *42*, 295.
- [22] C. Lu, J. Dai, N. Dong, Y. Zhu, Z. Xiong, *Plasma Processes Polym.* **2020**, *17*, 1069.
- [23] M. J. Pavlovich, D. S. Clark, D. B. Graves, *Plasma Sources Sci. Technol.* **2014**, *23*, 065036.
- [24] Z. Zou, R. Han, C. Lu, Z. Xiong, *Plasma Processes Polym.* **2020**, *18(1)*, e2000139.
- [25] K. G. Kerr, A. M. Snelling, *J. Hosp. Infect.* **2009**, *73*, 338.
- [26] D. Monti, L. Saccomani, P. Chetoni, S. Burgalassi, S. Tampucci, F. Mailland, *Br. J. Dermatol.* **2011**, *165*, 99.
- [27] L. Nogueiras-Nieto, J. L. Gómez-Amoza, M. B. Delgado-Charro, F. J. Otero-Espinar, *J. Controlled Release* **2011**, *156*, 337.
- [28] M. B. Shinn, *Ind. Eng. Chem., Anal. Ed.* **1941**, *13*, 33.
- [29] G. B. K. Hemal B Gunt, *J. Cosmet. Sci.* **2007**, *58*, 1.
- [30] K. Oehmigen, M. Hähnel, R. Brandenburg, C. Wilke, K. D. Weltmann, T. vonWoedtke, *Plasma Processes Polym.* **2010**, *7*, 250.
- [31] P. Kakkar, B. Madhan, G. Shanmugam, *SpringerPlus* **2014**, *3*, 596.
- [32] L. L. Perissinotti, G. Leitus, L. Shimon, D. Estrin, F. Doctorovich, *Inorg. Chem.* **2008**, *47*, 4723.
- [33] F. Kogelheide, K. Kartaschew, M. Strack, S. Baldus, N. Metzler-Nolte, M. Havenith, P. Awakowicz, K. Stapelmann, J.-W. Lackmann, *J. Phys. D: Appl. Phys.* **2016**, *49*, 084004.
- [34] M. J. Finnen, A. Hennessy, S. McLean, Y. Bisset, R. Mitchell, I. L. Megson, R. Weller, *Br. J. Dermatol.* **2007**, *157*, 494.
- [35] E. A. J. Bartis, P. Luan, A. J. Knoll, D. B. Graves, J. Seog, G. S. Oehrlein, *Plasma Processes Polym.* **2016**, *13*, 410.
- [36] P. Lukes, E. Dolezalova, I. Sisrova, M. Clupek, *Plasma Sources Sci. Technol.* **2014**, *23*, 015019.

How to cite this article: Z. Xiong, R. Huang, Y. Zhu, K. Luo, M. Li, Z. Zou, R. Han, *Plasma Processes Polym.* **2021**, e2000204. <https://doi.org/10.1002/ppap.202000204>